Measuring the refolding of β-sheets with different turn sequences on a nanosecond time scale

Rita P.-Y. Chen[†‡], Joseph J.-T. Huang[†§], Hsin-Liang Chen[¶‖], Howard Jan[†], Marappan Velusamy[†], Chung-Tien Lee[†], Wunshain Fann[¶‖], Randy W. Larsen[††], and Sunney I. Chan[†§‡‡]

Institutes of [†]Chemistry and [¶]Atomic and Molecular Sciences, Academia Sinica, Taipei 115, Taiwan, Republic of China; Departments of [§]Chemistry and [‖]Physics, National Taiwan University, Taipei 106, Taiwan, Republic of China; and [††]Department of Chemistry, University of South Florida, Tampa, FL 33620-5250

Edited by William F. DeGrado, University of Pennsylvania School of Medicine, Philadelphia, PA, and approved March 19, 2004 (received for review August 4, 2003)

Whether turns play an active or passive role in protein folding remains a controversial issue at this juncture. Here we use a photolabile cage strategy in combination with laser-flash photolysis and photoacoustic calorimetry to study the effects of different turns on the kinetics of β-hairpin refolding on a nanosecond time scale. This strategy opens up a temporal window to allow the observation of early kinetic events in the protein refolding process at ambient temperature and pH without interference from any denaturants. Our results provide direct evidence demonstrating that even a one-residue difference in the turn region can change the refolding kinetics of a peptide. This observation suggests an active role for turn formation in directing protein folding.

Reverse turns, with the ability of significantly restricting the conformational space available to the folding polypeptide chain and bringing distant parts of the chain into proximity, have long been suggested to play an important role in the initiation of protein folding (1, 2). In proteins, turns can play an important role in determining the structural stability as well as the details of the folding pathway (3–7). Although changes in the sequence of the turn or loop region can alter thermal stability and folding kinetics, there are mutations that remain tolerant of the change, depending on the role of the turn or the loop formation in the overall folding process. Several peptide models with a basic hairpin structure have been used to examine the relationship between turn sequence and turn conformation. They are either designed peptides (8–13) or short peptide segments adopted from protein sequences like ubiquitin (14–17) and the protein G B1 domain (18, 19). From these studies, there is little doubt that turn residues determine the conformation and stability of β-hairpins. However, although it has been proven that turns can indeed affect the equilibrium states of peptides, there have been only a few studies directed toward the effect of turns on kinetic properties. The paucity of data in this matter is perhaps due to the limitation of techniques in the detection of very fast events involving turns. The formation of hairpins is a very rapid process. It occurs much faster than the dead time of standard stopped-flow mixing devices (1 ≈ 2 ms) or that of the continuous-flow method (>45 μs) (20–22), and therefore folding is lost in the burst phase (missing amplitude) of the kinetic traces recorded by using these methods. On the other hand, time-resolved infrared spectroscopy and fluorescence spectroscopy in response to laser-induced temperature jump, which can quickly perturb the temperature of the system and hence the equilibrium between folded and unfolded states, have been successfully applied to the study of the rapid refolding of β-hairpins (23–25). Direct observation of the folding of peptides with different turns, however, remains elusive.

Here, we present a new method to initiate and interrogate rapid peptide refolding in real time. The strategy is based on the development of the compound 3′,5′-dimethoxybenzoin as a photolabile linker to modify and disrupt the structures of peptides (26–29). The 3′,5′-dimethoxybenzoin acetate can be photolyzed rapidly ($\approx 10^{-10}$·s^{-1}) by 308- to 366-nm light with a quantum yield of ≈0.64 to cleave the linker in the modified peptide. The photolyzed product, a 2-phenyl-5,7-dimethoxybenzofuran, is inert to further chemistry. Thus, the 3′,5′-dimethoxybenzoin is an ideal candidate for a phototrigger to initiate rapid peptide refolding.

Because cyclization is more likely to be successful in disrupting protein structure, a designed derivative, bromoacetyl-carboxymethoxy benzoin (BrAcCMB), is used to cyclize peptides in our studies (30). The reaction scheme is shown in Fig. 1. The carboxyl group of BrAcCMB is coupled to the N-terminal amino group of the peptide by solid-phase peptide synthesis. A cysteine residue in the polypeptide chain is selectively deprotected, whereas the side chains of the other residues remain protected. The free thio group can then react with the bromo group under basic conditions to cyclize the peptide. The cyclized peptide is cleaved from the resin and purified. Because the structure of the cyclized peptide is different from the native structure, upon irradiation, the photolabile linkage is broken and the linearized peptide chain containing the thioether analog of glutamate residue begins to refold. Because the photolabile linker is cleaved within a time scale of 100 ps, in principle it is possible to follow the reformation of secondary and tertiary structures in peptides and proteins on a nanosecond time scale. Note that no denaturant needs to be involved in this experiment so that the possible interference of external denaturants on the refolding process does not have to be addressed. Hansen *et al.* (30) have successfully applied this strategy to study the early kinetic events in the refolding process of the villin headpiece.

In this study, our target peptide is the three-stranded β-sheet first reported by Schenck and Gellman (31). The sequence of the peptide is: V F I T S ^{D}P G K T Y T E V ^{D}P G O K I L Q, where O stands for ornithine. We use this peptide as our model system instead of the two-stranded β-hairpin because of its excellent water solubility. Isolated β-hairpins are prone to aggregate because the forces that drive the intramolecular strand association can lead to the intermolecular aggregation as well. To adapt the cyclization strategy to the present problem, Glu-12 is replaced by a cysteine to facilitate the cyclization within the first hairpin of the β-sheet.

Earlier studies from this laboratory have shown that mutating the D form proline to aspartate [peptide with ^{D}P-6 to D mutation (P6D) mutation] can change the turn type from a four- to a five-residue turn and alter the side-chain pairings between the

This paper was submitted directly (Track II) to the PNAS office.

Abbreviations: TOCSY, total correlation spectroscopy; MALDI, matrix-assisted laser desorption ionization; E12C, peptide with E-12 to C mutation; c-E12C, cyclized E12C peptide; P6D, peptide with ^{D}P-6 to D mutation; P6DE12C, peptide with ^{D}P-6 to D and E-12 to C mutations; c-P6DE12C, cyclized P6DE12C peptide.

[‡]Present address: Institute of Biological Chemistry, Academia Sinica, Taipei 115, Taiwan, Republic of China.

[‡‡]To whom correspondence should be addressed. E-mail: chans@chem.sinica.edu.tw.

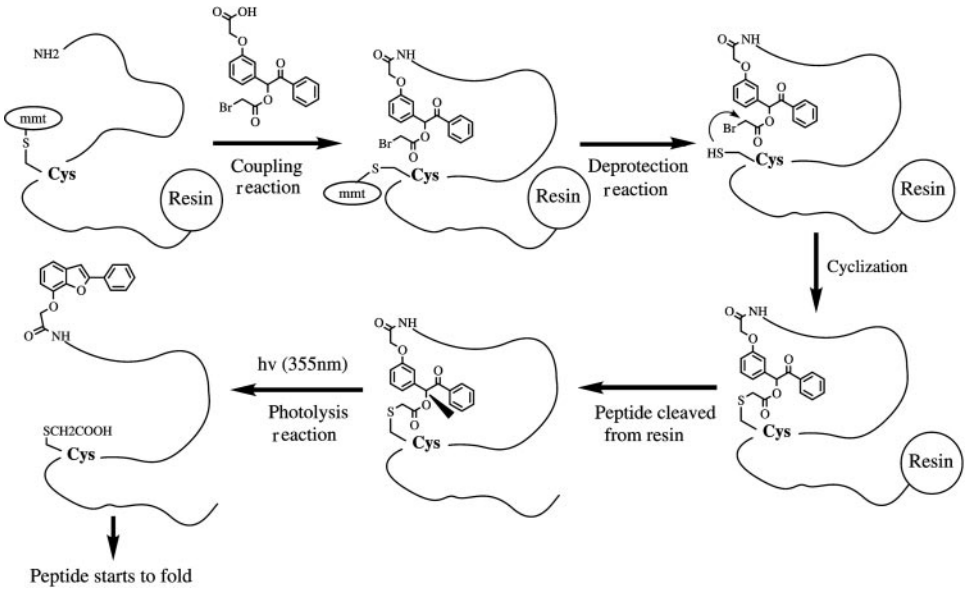

Fig. 1. Reaction scheme for peptide cyclization using the benzoin photolabile-linker strategy.

first two strands (11). The resulting frame shift is to accommodate the energetically disfavored S-D-G-K turn sequence by replacing it with the T-S-D-G-K turn. This mutation not only alters the strand register but also decreases the overall structural stability of the mutant peptide. Here, the peptide with the S-^{D}P-G-K turn and the peptide with the T-S-D-G-K turn are cyclized with the aid of our photolabile linker, and we have studied the manner in which these two turn sequences influence the kinetics of recovery of the hairpin structure by photoacoustic calorimetry (32, 33) (Fig. 2).

Methods

Peptide Synthesis. The peptides, peptide with E-12 to C mutation (E12C) (sequence V F I T S ^{D}P G K T Y T C V ^{D}P G O K I L Q), P6D (sequence V F I T S D G K T Y T E V ^{D}P G O K I L Q) and peptide with ^{D}P-6 to D and E-12 to C mutations (P6DE12C) (sequence V F I T S D G K T Y T C V ^{D}P G O K I L Q) were synthesized by the batch fluorenylmethoxycarbonyl(Fmoc)-polyamide method on a PS3 peptide synthesizer (Rainin Instruments). Rink amide AM resin from Nova Biochem was used as the solid support. Fmoc-Cys(mmt)-OH was used because the methoxytrityl (mmt) protecting group can be cleaved under mildly acidic condition. To synthesize the cyclized peptide, bromoacetyl-carboxymethoxy benzoin was coupled to the N-terminal end of the polypeptide chain. After coupling was completed, the resin was treated in 1% trifluoroacetic acid/5% triisopropylsilane in dichloromethane to remove the mmt group. The cyclization was performed on resin under basic conditions. The cyclized peptides, denoted peptide with E-12 to C mutation (c-E12C) and cyclized P6DE12C peptide (c-P6DE12C), were cleaved from the resin, purified, and identified as described in published procedures (11).

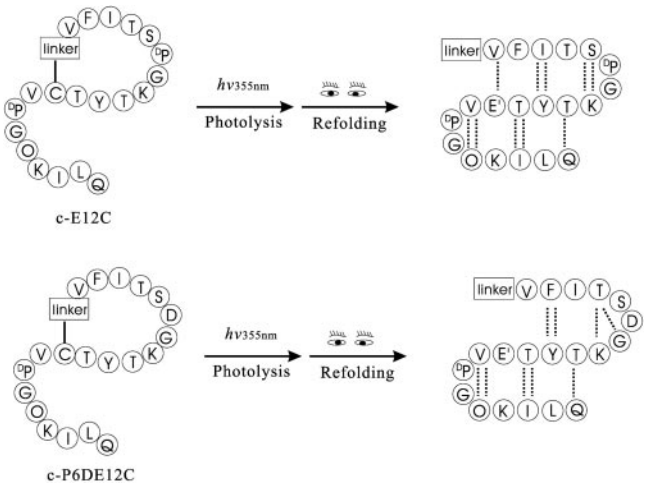

Fig. 2. Experimental design. Bromoacetyl-carboxymethoxy benzoin was used as a linker to cyclize the peptides. E′ represents the thio analogue of glutamate residue produced after photolysis.

CD Spectroscopy. CD spectra were recorded on a π^* CD spectrometer (Applied Photophysics, Surrey, U.K.). Peptides were dissolved in water. The CD spectra of the samples were recorded in a 1-mm cell, between 200 and 300 nm, at room temperature. A scan interval of 1 nm with an integration of 200,000 points was used. The spectrum of water was collected and subtracted automatically. To record the spectra of the photolyzed peptides, the peptide samples were irradiated in a "merry-go-round" photoreactor PR-2000 (Pan-Chum, Taiwan, Republic of China) equipped with 16-UV lamps at 352 nm for 400 seconds before collecting the CD spectra.

NMR Spectroscopy. All NMR spectra were recorded on a Bruker (Billerica, MA) AM 500 NMR spectrometer. Samples were dissolved in deionized water (H_2O/D_2O = 9/1). The concentrations of the peptide samples were ≈3 mM. 1/500 volume of sodium 3-(trimethylsilyl)-propionic-2, 2, 3, 3-d_4 acid solution (0.75% in D_2O) was added as an internal reference. 2D total correlation spectroscopy (TOCSY) and nuclear Overhauser effect spectroscopy (NOESY) were recorded by using standard phase-cycling sequences at 293 K. Usually, spectra were acquired with 2,000 data points in the direct dimension and 512 increments in the indirect dimension. Generally, 128 scans were collected per increment. Eighty-millisecond mixing time in TOCSY and 300-ms mixing time in NOESY were used. Data were processed by XWINNMR software (Bruker). The shifted square sine bell window functions in both dimensions were

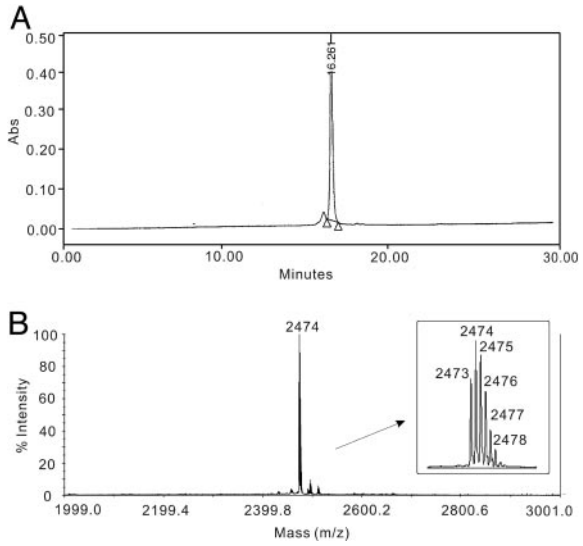

Fig. 3. (*A*) HPLC chromatograph of c-E12C. Peptides were eluted from a reverse-phase C18 column with a linear gradient of 0–100% acetonitrile in the presence of 0.1% trifluoroacetic acid over a period of 30 min. (*B*) MALDI-mass spectrum of c-E12C. The calculated monoisotopic mass of c-E12C is 2,472.2 atomic mass units.

applied for all spectra. The ANSIG program (Ver. 3.3) was used to assign the spectra (34).

Laser-Flash Photolysis. Photo excitation was achieved by the 355-nm third harmonic of a Q-switch Nd-YAG laser (New Wave Research, Fremont, CA). The laser pulse width was ≈5 ns, and the repetition rate was 2 Hz. The typical power used in the experiment was a few microjoule.

Photoacoustic Calorimetry. Peptides were dissolved in distilled water until the OD_{355} reached 0.05. The sample was kept in a quartz cuvette with 1-cm path length. The cuvette holder (Quantum Northwest, Spokane, WA) was temperature controlled at 20 ± 0.5°C. The photoacoustic pressure wave generated after laser irradiation was detected by using a microphone (PZT piezoelectric transducer) with 1-MHz bandwidth (General Electric Panametrics V-103). The microphone was mounted on the side wall of the cuvette. The signals from the microphone were sent to a preamplifier (General Electric Panametrics 5670, 40-dB gain) and recorded by a digital oscilloscope (TDS 784D, Tektronix). The signals from 50 laser shots were averaged.

Data Analysis. As noted earlier, the observed signal, $S(t)$, is the convolution of the heat source function, $H(t)$, with the instrument response function, $R(t)$.

$$S(t) = \int R(t\text{-}t')\, H(t')dt' \qquad [1]$$

The instrument response function, essential for deconvolution, was obtained by recording the signal from a reference compound (Eq. **1**). The reference compound name is Fe(III)meso-tetra(4-sulfonatophenyl)-porphine chloride. An ideal reference compound would convert all of the absorbed photon energy into heat in nanoseconds. For our peptides, we assume $H(t) = \Sigma\phi_i\, e^{-t/\tau i}$ (ϕ_i and τ_i are the preexponential factor and decay lifetime, respectively, for the ith component in a sum of exponentials). Optimized fitting was performed by using SOUND ANALYSIS software provided by Quantum Northwest. The $S(t)$ and $R(t)$ were normalized according to their absorbance for the fitting process.

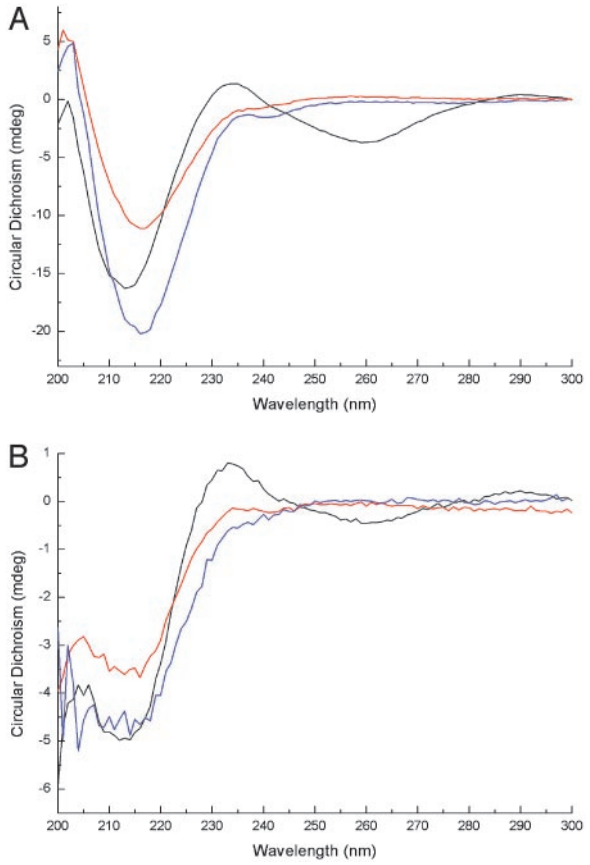

Fig. 4. (*A*) CD spectra of c-E12C (black) and photolyzed c-E12C (red) compared with the wild-type peptide (blue). Peptides were dissolved in water to a final concentration of 35 μM. (*B*) CD spectra of c-P6DE12C (black) and photolyzed c-P6DE12C (red) compared with the P6D peptide (blue). Peptides were dissolved in water to a final concentration of 10 μM.

Our current apparatus could measure enthalpy changes from 30 ns to 5 μs. The shortest time cutoff was set by the measurable phase shift from the acoustic signal. The longest time limit was determined by the reflected acoustic wave.

Results

Examining the Structural Alteration of the Peptides After Cyclization by CD Spectroscopy and NMR Spectroscopy. The peptides E12C and P6DE12C were cyclized with the linker as described above. The purity of the cyclized peptide was demonstrated by the HPLC chromatograph and identified by its mass spectrum (Fig. 3).

The CD spectra of the wild-type peptide and the cyclized peptide c-E12C are compared in Fig. 4*A*. The appearance of a negative ellipticity in the near UV region of the spectrum of c-E12C, and that of the negative ellipticity in the far UV region was blue shifted from 216 to 213 nm upon cyclization, suggested that the structure of the peptide was not native-like and that some nonnative hydrophobic interactions of the aromatic residues had taken place after cyclization. On the other hand, the CD spectrum of the photolyzed c-E12C was very similar to that of the wild-type peptide, evidence that the cyclized peptide could refold back to its native structure after cleavage of the linker. The amplitude decrease in the CD spectrum of the photolyzed peptide was due to the undesired hydrolysis after extended irradiation.

Similarly, the CD spectra of the c-P6DE12C before and after photolysis are compared with that of the peptide P6D in Fig. 4*B*. Because the negative ellipticity at 216 nm originated from the

BIOPHYSICS

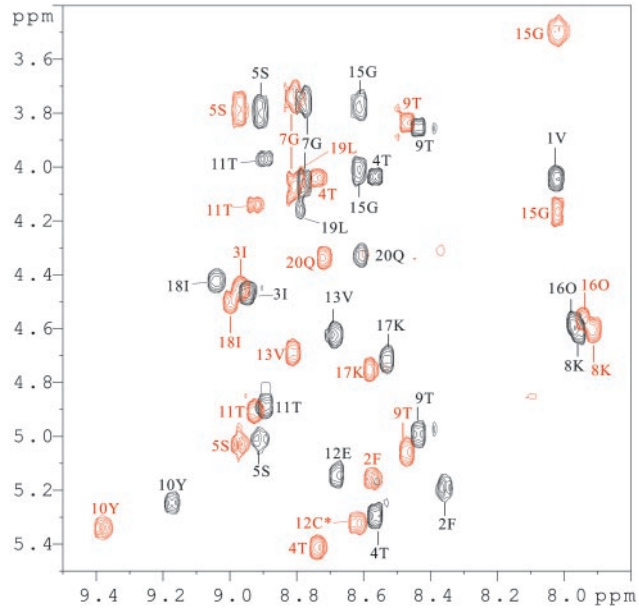

Fig. 5. Fingerprint regions of the 2D-TOCSY spectra of c-E12C (red contours) and the wild-type peptide (black contours). C* represents the cysteine residue participating in the cyclization.

two ^{D}P-G turns, replacing ^{D}Pro with Asp induced a blue shifting of the spectrum to 213 nm for all of the peptides with this mutation. The similar negative ellipticity in the near UV region suggested that c-P6DE12C possessed the same nonnative hydrophobic interactions as the c-E12C. Thus, the structures of c-E12C and c-P6DE12C were perturbed from their respective native structures by the constraints introduced by the cyclization, but both partially unfolded peptides could refold back to their native structures after photolysis. In light of this, we could compare the effects of the different turn sequences on the refolding kinetics.

2D TOCSY and nuclear Overhauser effect spectroscopy (NOESY) spectra of the c-E12C and the wild-type peptides were also recorded and compared. It was not surprising that some interstrand NOEs were still evident in the NOESY spectra because our cyclization site occurred near the end of the first hairpin. Cyclization actually pulled the two ends of the first hairpin closer to each other. However, from a comparison of the H^{α} and HN chemical shifts of individual residues, it was clear that cyclization did change the peptide structure. In Fig. 5, we have superimposed the fingerprint regions of the 2D TOCSY spectra of c-E12C and the wild-type peptide. The H^{α} and HN chemical shifts of c-E12C are clearly different from those of the wild-type peptide, especially for residues F2, T4, Y10, E12, V13, G15, I18, and L19, further confirming that the cyclized peptide is truly in a nonnative state, as suggested by the CD studies.

Refolding Kinetics of the Peptides by Photoacoustic Calorimetry. Although photoacoustic calorimetry has been widely used to study photoinitiated nonradiative process in solution, the application of this method to protein folding is quite new (30, 33). The schematic of a photoacoustic calorimetry apparatus is shown in Fig. 6. The principle of photoacoustic calorimetry is relatively simple. The molecule under study absorbs a photon, and the light absorption triggers a chemical event that leads to heat release or absorption and possibly a conformational event. Expansion or contraction of the solvent induced by the heat of the reaction and/or the volume change associated with the conformational

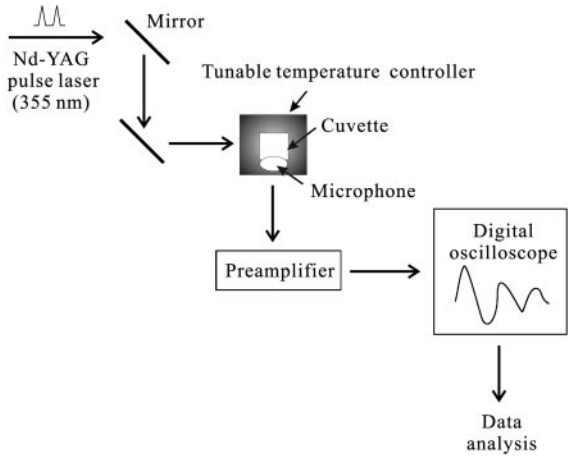

Fig. 6. Schematic setup of photoacoustic calorimeter apparatus.

event generate a pressure wave, which is propagated through the solution to a piezoelectric transducer for acoustic detection.

The photoacoustic signals of the peptide c-E12C and c-P6DE12C after photolysis by laser irradiation are displayed in Figs. 7 and 8, respectively. After deconvolution, the amplitude and the time constant of each phase were obtained. The experiments were repeated at least three times and the results

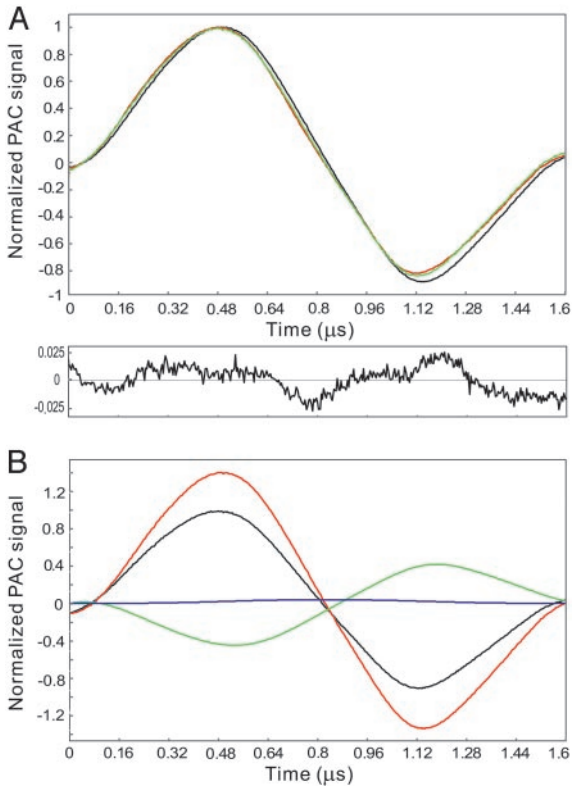

Fig. 7. (*A Upper*) The photoacoustic wave generated by laser irradiation of c-E12C. The signals from the peptide sample and the reference compound are shown in red and black, respectively. The green wave is the simulated wave for the sample derived from the results of the deconvolution (see *B*). (*Lower*) The corresponding residuals are shown. (*B*) Shown here are the overall simulated curve (black) together with the three deconvoluted component waves associated with the linker breaking event (red), the folding event (green), and background (blue). Amplitudes and time constants of the component waves are: $\phi_1 = 1.46$, $\tau_1 = 1$ fs; $\phi_2 = -0.49$, $\tau_2 = 38$ ns; and $\phi_3 = 154$, $\tau_3 = 3.59$ ms.

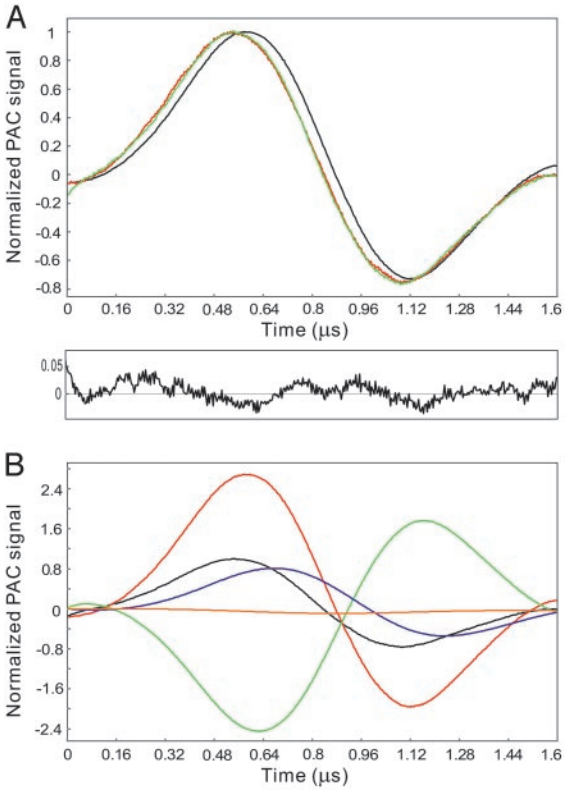

Fig. 8. (*A Upper*) The photoacoustic wave generated by laser irradiation of c-P6DE12C. The signals from the peptide sample and the reference compound are shown in red and black, respectively. The green wave is the simulated wave for the sample derived from the results of the deconvolution (see *B*). (*Lower*) The corresponding residuals are shown. (*B*) Shown here is the overall simulated curve (black) together with the four deconvoluted component waves associated with the linker breaking event (red), the first folding event (green), the second folding event (blue), and the background (orange). Amplitudes and time constants of the component waves are: $\phi_1 = 2.18$, $\tau_1 = 1$ fs; $\phi_2 = -1.57$, $\tau_2 = 41$ ns; $\phi_3 = 0.48$, $\tau_3 = 148$ ns; and $\phi_4 = -775$, $\tau_4 = 3.38$ ms.

were averaged. For c-E12C, all of the data were best fitted by three components. The time constant of the first component was fixed to a very short time (1 fs) in the deconvolution and corresponded to the instrumental response function. The positive amplitude of the first component ($\phi_1 = 1.46$) corresponded to the heat released during the photocleavage of the benzoin linker. The second component described an event occurring after cleavage of the linker. Our data indicated that the refolding of c-E12C from its initial state immediately after cleavage of the linker was completed with a time constant ≈40 ns at 20°C. The negative amplitude ($\phi_2 = -0.49$) suggested that the refolding was a very fast endothermic (entropy-driven!) reaction (assuming that the contribution from the volume change of the peptide during the refolding process was relatively small). There must be a corresponding increase in the accessible peptide conformational states after the cyclization constraint was removed. A very long time constant was set for the third component in the beginning of the fitting to represent the background signal to obtain perfect fitting.

Interestingly, one additional phase was observed for c-P6DE12C after cleavage of the photolabile linker. All of the data were best fitted by four components. Apart from the first and the fourth components, corresponding to the heat released during photocleavage of the caged peptide and the background signal mentioned earlier, respectively, two other processes were resolved in the photoacoustic experiment. The time constant for

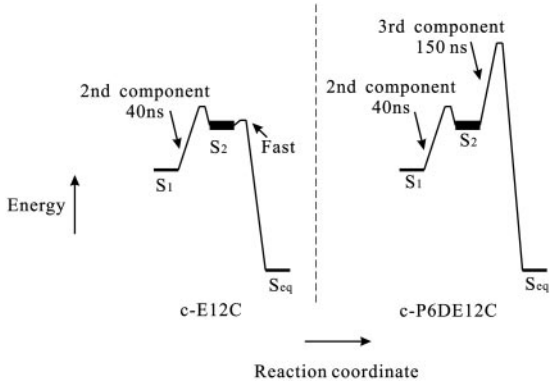

Fig. 9. Schematics of the refolding processes for c-E12C and c-P6DE12C after photolysis as described by simple energy diagrams.

the second component was ≈40 ns, identical to the second component observed in the refolding of c-E12C. Most importantly, the time constant associated with the third component was ≈150 ns. This additional component exhibited positive amplitude ($\phi_3 = 0.48$), indicating that it was associated with an exothermic event. Apparently, the peptide with a T-S-D-G-K turn needed a longer time to return to its equilibrium state than the peptide with the more favored S-^{D}P-G-K turn. Thus, the turn region in the β-sheet plays a key role in guiding the subsequent assembly of the structure during the early stages of the folding process.

Schematics of the observed processes for the two peptides are depicted in Fig. 9. The relative energies of the intermediates involved in the folding are shown according to their reaction coordinates, and the energy bandwidth is used to denote the density of conformational states associated with each intermediate.

Discussion

In our studies, both peptides were constrained in the same initial state S_0 by cyclization. Because this state was formed by forcing the peptide into a constrained structure with the use of covalent bonds, it could not be shown in the Fig. 9. However, the state formed immediately after the breaking of the linker could be shown, and this state is depicted by S_1. Because S_1 was initially stabilized by some nonnative hydrophobic interactions as indicated by the presence of a near-UV CD band, the transition of the peptide from S_1 and S_2 is expected to be enthalpically uphill, and hence the conformational rearrangement must be entropically driven. Accordingly, the two peptides absorbed heat from the surroundings (solvent) during this step. Interestingly, this $S_1 \rightarrow S_2$ step proceeded with the same time constant of ≈40 ns for both peptides. Although the process is approaching the time resolution of our photoacoustic calorimetry apparatus (≈30 ns), the difference in folding kinetics between the two peptides is distinct due to the existence of an additional folding phase.

After the $S_1 \rightarrow S_2$ step, the peptide with the ^{D}Pro-G turn underwent a rapid "collapse" toward its equilibrium structure (S_{eq}). On the other hand, the peptide with the D-G sequence went through an additional rearrangement process, an exothermic one driven by the heat released from hydrophobic annealing and hydrogen-bond formation before its "collapse" toward its own equilibrium structure. The time constant associated with this step was ≈150 ns.

The peptides with different turn sequences possess different side-chain pairings, as shown in Fig. 2. Evidently, the S-D-G-K sequence cannot form a turn as strong as the ^{D}Pro-G turn, and it is necessary to give up one residue to stabilize the turn. It is possible that a "turn" was not initially formed with the final set

of side-chain pairings during the refolding of the hairpin with the Asp mutation. If a different set of side-chain pairings were used, some readjustments or rearrangement of the side-chain pairings would have to be made before the peptide could continue on its final "collapse" toward the equilibrium structure. In any case, it is tantalizing that our method can be used to observe different folding kinetics from peptides with a difference of only one-residue.

The early kinetic events that we have observed for the two β-sheets in the present study are extremely rapid, albeit slower than the corresponding refolding of α helices. The measured time scales are of the same order as those noted in the refolding of β-hairpins. Recently, Xu *et al.* (25) have studied the folding kinetics of a short designed hairpin peptide by time-resolved infrared spectroscopy after laser-induced temperature jump and reported a folding time of $\approx$0.8 μs. Maness *et al.* (24) have also used similar techniques to study the folding of cyclic β-hairpin peptides and concluded that their folding rates were two orders faster than that of a linear peptide. Because our caged β-sheet peptides are already partially structured as in the case of the cyclic β-hairpin peptides of Maness *et al.* (24), the kinetic events that we have measured most likely correspond to conformational rearrangements, rather than the overall collapse of the β-sheet from a random ensemble of unstructured states. Indeed, Muñoz *et al.* (23) have studied the folding kinetics of one of the hairpin peptides from the protein GB1 domain after laser-induced temperature jump and have shown that the refolding of the linear hairpin from the random ensemble of unfolded states occurs in 6 μs at room temperature, a substantially longer time scale. On the other hand, there is also a fundamental difference between the turn sequences of the β-sheets examined in our study and that studied in the work of Muñoz *et al.* (23). As type II′ turns, the folding of the β-sheets in our study is more likely nucleated at the turn rather than by hydrophobic collapse. Whether "the folding of a hairpin or β-sheet nucleates at the turn, followed by zipping of the structure," as suggested by Muñoz *et al.* (23), or "the β-sheet is nucleated by hydrophobic collapse followed by rearrangements to produce a native-like topology," as proposed by Dinner *et al.* (35), the early kinetic events that we are observing here are expected to be prominent during the early stages of protein refolding, and in principle, any errors in this step could deleteriously affect subsequent steps in the refolding of a protein. In particular, the nucleation of improper turns could contribute to undesirable exposure of hydrophobic surfaces during the refolding process and kinetically enhance the irreversible formation of insoluble aggregates. Finally, although our approach does not allow us to monitor the global refolding in our experiments because of the initial cyclization constraint limiting the peptide to a subset of conformational space, the method has the distinct advantage that the experiment begins with the same well-defined initial state and allows direct observation and comparison of the structural change of the peptides with different sequences from the same initial state in real time.

Conclusion

We have used a photolabile linker to cyclize a hairpin and measured its refolding rate after photocleavage of the linker with a nanosecond laser pulse by using photoacoustic calorimetry. In this work, we have monitored and compared the effects of two turn sequences on the refolding of a hairpin on the nanosecond time scale. We have found that a one-residue difference in the turn region not only can change the stability and the equilibrium structure of the hairpin but can also affect the folding kinetics. The latter is usually not detected in traditional folding studies. Moreover, it is difficult to follow the fast folding kinetics of short peptides by spectroscopic methods. By measuring the heat released or absorbed during the refolding reaction, the introduction of a foreign chromophore is not required. The method is particularly useful for detecting local sequence effects on the early kinetic events of protein folding under ambient conditions without resorting to temperature, pH, or pressure jumps and/or adding denaturants to the system.

We thank Prof. Tien-Yau Luh, Dr. Hsian-Rong Tseng, and Dr. Joern Wirsch in the Department of Chemistry at National Taiwan University for assistance in the synthesis of our linker. This work was supported by a program project grant from Academia Sinica as well as by Grant NSC 91-2119-M-001-012 from the National Science Council, Taiwan.

1. Lewis, P. N., Momany, F. A. & Scheraga, H. A. (1971) *Proc. Natl. Acad. Sci. USA* **68,** 2293–2297.
2. Zimmerman, S. S. & Scheraga, H. A. (1977) *Proc. Natl. Acad. Sci. USA* **74,** 4126–4129.
3. Kim, K. Y. & Frieden, C. (1998) *Protein Sci.* **7,** 1821–1828.
4. Chen, P. Y., Gopalacushina, B. G., Yang, C. C., Chan, S. I. & Evans, P. A. (2001) *Protein Sci.* **10,** 2063–2074.
5. Nauli, S., Kuhlman, B. & Baker, D. (2001) *Nat. Struct. Biol.* **8,** 602–605.
6. McCallister, E. L., Alm, E. & Baker, D. (2000) *Nat. Struct. Biol.* **7,** 669–673.
7. Zhou, H. X., Hoess, R. H. & DeGrado, W. F. (1996) *Nat. Struct. Biol.* **3,** 446–451.
8. de Alba, E., Rico, M. & Jimenez, M. A. (1999) *Protein Sci.* **8,** 2234–2244.
9. Ramírez-Alvarado, M., Blanco, F. J., Niemann, H. & Serrano, L. (1997) *J. Mol. Biol.* **273,** 898–912.
10. Stanger, H. E. & Gellman, S. H. (1998) *J. Am. Chem. Soc.* **120,** 4236–4237.
11. Chen, P. Y., Lin, C. K., Lee, C. T., Jan, H. & Chan, S. I. (2001) *Protein Sci.* **10,** 1794–1800.
12. deAlba, E., Jimenez, M. A. & Rico, M. (1997) *J. Am. Chem. Soc.* **119,** 175–183.
13. de Alba, E., Santoro, J., Rico, M. & Jimenez, M. A. (1999) *Protein Sci.* **8,** 854–865.
14. Searle, M. S., Williams, D. H. & Packman, L. C. (1995) *Nat. Struct. Biol.* **2,** 999–1006.
15. Haque, T. S. & Gellman, S. H. (1997) *J. Am. Chem. Soc.* **119,** 2303–2304.
16. Zerella, R., Chen, P. Y., Evans, P. A., Raine, A. & Williams, D. H. (2000) *Protein Sci.* **9,** 2142–2150.
17. Zerella, R., Evans, P. A., Ionides, J. M. C., Packman, L. C., Trotter, B. W., Mackay, J. P. & Williams, D. H. (1999) *Protein Sci.* **8,** 1320–1331.
18. Blanco, F. J. & Serrano, L. (1995) *Eur. J. Biochem.* **230,** 634–649.
19. Blanco, F. J., Rivas, G. & Serrano, L. (1994) *Nat. Struct. Biol.* **1,** 584–590.
20. Shastry, M. C., Luck, S. D. & Roder, H. (1998) *Biophys. J.* **74,** 2714–2721.
21. Shastry, M. C. & Roder, H. (1998) *Nat. Struct. Biol.* **5,** 385–392.
22. Park, S. H., Shastry, M. C. & Roder, H. (1999) *Nat. Struct. Biol.* **6,** 943–947.
23. Muñoz, V., Thompson, P. A., Hofrichter, J. & Eaton, W. A. (1997) *Nature* **390,** 196–199.
24. Maness, S. J., Franzen, S., Gibbs, A. C., Causgrove, T. P. & Dyer, R. B. (2003) *Biophys. J.* **84,** 3874–3882.
25. Xu, Y., Oyola, R. & Gai, F. (2003) *J. Am. Chem. Soc.* **125,** 15388–15394.
26. Sheehan, J. C., Wilson, R. M. & Oxford, A. W. (1971) *J. Am. Chem. Soc.* **93,** 7222–7228.
27. Rock, R. S. & Chan, S. I. (1998) *J. Am. Chem. Soc.* **120,** 10766–10767.
28. Rock, R. S. & Chan, S. I. (1996) *J. Org. Chem.* **61,** 1526–1529.
29. Stowell, M. H. B., Rock, R. S., Rees, D. C. & Chan, S. I. (1996) *Tetrahedron Lett.* **37,** 307–310.
30. Hansen, K. C., Rock, R. S., Larsen, R. W. & Chan, S. I. (2000) *J. Am. Chem. Soc.* **122,** 11567–11568.
31. Schenck, H. L. & Gellman, S. H. (1998) *J. Am. Chem. Soc.* **120,** 4869–4870.
32. Braslavsky, S. E. & Heibel, G. E. (1992) *Chem. Rev.* **92,** 1381–1410.
33. Abbruzzetti, S., Crema, E., Masino, L., Vecli, A., Viappiani, C., Small, J. R., Libertini, L. J. & Small, E. W. (2000) *Biophys. J.* **78,** 405–415.
34. Kraulis, P. J. (1989) *J. Magn. Reson.* **24,** 627–633.
35. Dinner, A. R., Lazaridis, T. & Karplus, M. (1999) *Proc. Natl. Acad. Sci. USA* **96,** 9068–9073.